AD-A192 203 HIGHER FREQUENCY AMBIENT NOISE IN THE ARCTIC OCEAN(U) 1/1
SCIENCE APPLICATIONS INTERNATIONAL CORP COLLEGE STATION
TX J K LEWIS ET AL. JAN 88 SAIC-87/1068
UNCLASSIFIED N00014-87-C-0115 F/G 20/1 NL

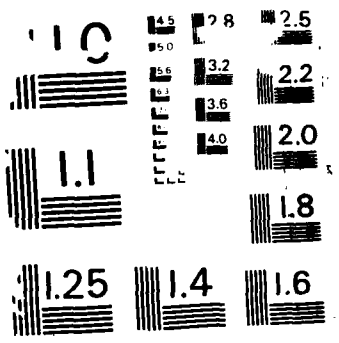

TEST CHART
NATIONAL BUREAU OF STANDARDS

(2)

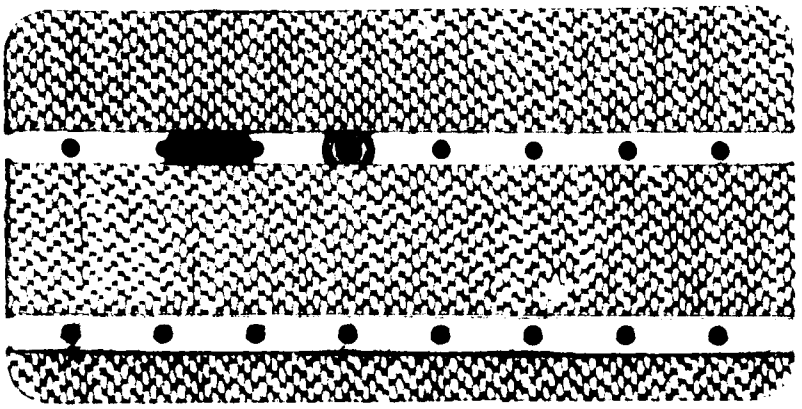

SAIC™

Science Applications International Corporation

HIGHER FREQUENCY AMBIENT NOISE

IN THE ARCTIC OCEAN

SAIC
Science Applications International Corporation

1304 Deacon
College Station, Texas 77840

James K. Lewis
Warren W. Denner

A Report to the Office of Naval Research
N00014-87-C-0115
SAIC-87/1868

January 1988

Post Office Box 1303, 1710 Goodridge Drive, McLean, Virginia 22102. (703) 821-4300

Unclassifed

SECURITY CLASSIFICATION OF THIS PAGE

ADA192203

REPORT DOCUMENTATION PAGE

1a. REPORT SECURITY CLASSIFICATION Unclassifed	1b. RESTRICTIVE MARKINGS None
2a. SECURITY CLASSIFICATION AUTHORITY	3. DISTRIBUTION / AVAILABILITY OF REPORT Approved for public Release; Distribution unlimited
2b. DECLASSIFICATION / DOWNGRADING SCHEDULE	
4. PERFORMING ORGANIZATION REPORT NUMBER(S) SAIC-87/ 1868	5. MONITORING ORGANIZATION REPORT NUMBER(S)
6a. NAME OF PERFORMING ORGANIZATION Science Applications Int'l Corp 6b. OFFICE SYMBOL (If applicable)	7a. NAME OF MONITORING ORGANIZATION Office of Naval Research
6c. ADDRESS (City, State, and ZIP Code) 1304 Deacon College Station, Tx 77840	7b. ADDRESS (City, State, and ZIP Code) 800 N. Quincy Street Arlington, Va. 22217
8a. NAME OF FUNDING / SPONSORING ORGANIZATION 8b. OFFICE SYMBOL (If applicable) ONR 1125AR	9. PROCUREMENT INSTRUMENT IDENTIFICATION NUMBER N00014-87-C-0115
8c. ADDRESS (City, State, and ZIP Code)	10. SOURCE OF FUNDING NUMBERS PROGRAM ELEMENT NO. 61153N; PROJECT NO.; TASK NO.; WORK UNIT ACCESSION NO

11. TITLE (Include Security Classification)

HIGHER FREQUENCY AMBIENT NOISE IN THE ARCTIC

12. PERSONAL AUTHOR(S)
James K Lewis, Warren W. Denner

13a. TYPE OF REPORT	13b. TIME COVERED	14. DATE OF REPORT (Year, Month, Day)	15. PAGE COUNT
Technical	FROM 1 Jan TO 31 Dec87	January 1988	25

16. SUPPLEMENTARY NOTATION

17. COSATI CODES			18. SUBJECT TERMS (Continue on reverse if necessary and identify by block number)
FIELD	GROUP	SUB-GROUP	

19. ABSTRACT (Continue on reverse if necessary and identify by block number)

Higher frequency (1000 Hz) arctic ambient noise episodes during non-summer months were used to study generating mechanisms. In most cases, thermal fracturing of sea ice was responsible. A suite of heating and cooling processes that relate to thermal fracturing of sea ice were considered. Numerical simulations with a daily heating cycle and no snow cover impli d that maximum noise levels occurred at 1900 hrs local. Radiational heat balances are more important than sensible heat flux in producing fracturing of sea ice. With snow cover, the amount of ice fracturing is reduced. A daily heating cycle produces maximum fracturing at 0300 to 0800 hrs local, a common feature seen in observed noise data. Simulations were made using observed Arctic Ocean solar radiation, air temperature, wind speed, albedo, and cloud cover from the spring of 1976. The agreement between the model ice fracturing parameter and the observed 1000 Hz noise levels was excellent. However, results indicate that blowing snow and ice fog may be additional factors in the heat flux balance of sea ice.

20. DISTRIBUTION / AVAILABILITY OF ABSTRACT	21. ABSTRACT SECURITY CLASSIFICATION
☒ UNCLASSIFIED/UNLIMITED ☐ SAME AS RPT. ☐ DTIC USERS	Unclassified
22a. NAME OF RESPONSIBLE INDIVIDUAL Robert Obrochta	22b. TELEPHONE (Include Area Code) 202-696-4118,9
	22c. OFFICE SYMBOL ONR 1125AR

DD FORM 1473, 84 MAR

83 APR edition may be used until exhausted.
All other editions are obsolete.

SECURITY CLASSIFICATION OF THIS PAGE

Unclassifed

The short space scales of higher frequency, arctic ambient noise are likely a result of spatial variations in snow cover. The short time scales of such noise are not only a result of multiple noise-generating processes but also changes in cloud and snow cover. Results indicate that thermal fracturing of sea ice can produce broad-band noise. There are clear examples of 32 Hz noise variations associated with thermal fracturing of sea ice.

Definition of Symbols

C - Fractional cloud cover.
c_I - Specific heat of ice.
C_p - Specific heat of air.
C_s - Bulk transfer coefficient for heat between ice and air.
e_L - Emissivity for ice.
e^* - Emissivity for air.
f - Oscillation frequency of ice temperature.
F - Thermal fracturing parameter of ice.
H - Ice thickness.
k - Thermal conductivity ($W\ m^{-1}\ °C^{-1}$).
S - Salinity (parts per thousand).
S_L - Linear gradient of noise level in space (pressure amplitude units per km).
t - Time.
T - Temperature of air or ice.
U - Wind speed.
α - Inverse of the e-folding depth of temperature fluctuations within ice.
ρ - Density of air, ice, or snow.
ω - Oscillation frequency of air temperature.

ABSTRACT

Higher frequency (1000 Hz) arctic ambient noise episodes during non-summer months were used to study generating mechanisms. In most cases, thermal fracturing of sea ice was responsible. A suite of heating and cooling processes that relate to thermal fracturing of sea ice were considered. Numerical simulations with a daily heating cycle and no snow cover implied that maximum noise levels occurred at 1900 hrs local. Radiational heat balances are more important than sensible heat flux in producing fracturing of sea ice. With snow cover, the amount of ice fracturing is reduced. A daily heating cycle produces maximum fracturing at 0300 to 0800 hrs local, a common feature seen in observed noise data. Simulations were made using observed Arctic Ocean solar radiation, air temperature, wind speed, albedo, and cloud cover from the spring of 1976. The agreement between the model ice fracturing parameter and the observed 1000 Hz noise levels was excellent. However, results indicate that blowing snow and ice fog may be additional factors in the heat flux balance of sea ice.

The short space scales of higher frequency, arctic ambient noise are likely a result of spatial variations in snow cover. The short time scales of such noise are not only a result of multiple noise-generating processes but also changes in cloud and snow cover. Results indicate that thermal fracturing of sea ice can produce broad-band noise. There are clear examples of 32 Hz noise variations associated with thermal fracturing of sea ice.

Definition of Symbols

C - Fractional cloud cover.
c_I - Specific heat of ice.
C_p - Specific heat of air.
C_s - Bulk transfer coefficient for heat between ice and air.
e_L - Emissivity for ice.
e^* - Emissivity for air.
f - Oscillation frequency of ice temperature.
F - Thermal fracturing parameter of ice.
H - Ice thickness.
k - Thermal conductivity (W m^{-1} $°C^{-1}$).
S - Salinity (parts per thousand).
S_L - Linear gradient of noise level in space (pressure amplitude units per km).
t - Time.
T - Temperature of air or ice.
U - Wind speed.
α - Inverse of the e-folding depth of temperature fluctuations within ice.
ρ - Density of air, ice, or snow.
ω - Oscillation frequency of air temperature.

TABLE OF CONTENTS

1. INTRODUCTION

A number of interesting and innovative concepts concerning arctic ambient noise have been developed recently. Specifically, noise generation through various modes of ice stress have been documented[1], and the general spatial and temporal characteristics of noise at various frequencies have been quantified[2]. Recent studies have also delved into the seasonal variations of the generation of noise by different sea ice processes[3]. From all this recent work, one factor has become quite evident: our knowledge of the generation of higher frequency (>300 Hz) noise in the arctic is considerably less complete than that of lower frequency (<100 Hz) noise.

Previous studies of higher frequency noise have yielded a few certain facts. The first deals with space and time scales. Higher frequency noise during the summer is mostly generated by sea ice motion[3]. The space and time scales are ~300 km and about 24 hrs, respectively, values that one would expect for motion-induced noise[2]. During the other seasons, higher frequency noise can have greater spatial variability (resulting in shorter space scales), and this is accompanied by a dramatic decrease in time scales. The shorter time scales for non-summer months (9-12 hrs) are taken as a reflection of multiple noise-generating mechanisms at frequencies >300 Hz.

The space scales of higher frequency can have a minimum of 170 km in fall and then increase to the order of 300 km in the spring and summer[2]. The increase through spring could be a reflection of the greater compactness and rigidity of the ice field. Also, the drop from 300 km during summer to 170 km during fall has been attributed to some degree to the spatial variations in the frozen state of the ice pack[3]. But the extremely short space scales during winter (order of 250 km) and spring do not appear to be logical. If the primary forcings are atmospheric, one would expect the scale of such forcings to be of the order of 500 km or more, even for temporally incoherent processes.

A second factor concerning higher frequency noise is its seemingly poor correlation with environmental parameters. During non-summer months, the horizontal movement of pack ice accounts for only 50% or less of the variance of higher frequency noise[3]. Of particular interest is the relationship between non-summer higher frequency noise and air temperature fluctuations. Milne[4] had found a close relationship between higher frequency noise and air temperature variations during the arctic spring. However, Lewis and Denner[3] found that a parameterization for sensible heat fluxes using air temperatures had no significant correlation with the corresponding fall and winter 1000 Hz noise signals under the ice. This implies that the heat flux through sea ice must be considered more thoroughly and exactly. Moreover, poor correlations may be an indication that we have yet to discover a significant mechanism for the generation of higher frequency noise.

This paper presents the results of a study of higher frequency noise episodes to determine specifics of the generation of such under-ice noise. We concentrated on non-summer months since these time periods are the least understood with respect to higher frequency noise generation and space and time scales. In particular, we examined those noise episodes which seemingly had no relationship with ice motion or wind stress events. These anomalous noise episodes were found to fall into two categories. The first had characteristics of large noise amplitudes but short time durations (0.6 to 1.25 days). These have been associated with the thermal microfracturing of the ice pack. The second category was smaller in noise amplitude but longer in time duration (1.75 days and greater). These noise anomalies were few and are similar to those associated with summer-time microfracturing of the ice pack due to motion. However, in some cases, we found no direct indication that these non-summer anomalies are motion induced.

Because of the importance of the higher frequency noise signatures due to thermal microfracturing, the propagation of a thermal wave in sea ice was also studied. It was found that fall and winter microfracturing can be a complex process involving the loss of heat through net longwave radiation. Sensible heat flux plays a minor roll. During spring, shortwave solar radiation into the ice, snow cover, and the longwave radiation from the ice and from the atmosphere combine to drive the thermal wave in the ice. However, this driving and the resulting microfracturing noise can be radically modified on a day-to-day basis as a result of cloud cover, blowing snow, etc.

2. THE DATA

The data used in this study were from the Arctic Ice Dynamics Joint Experiment (AIDJEX) which began in March 1975 and ended in May 1976. Four sites on the Beaufort Sea ice pack were initially manned, and were tracked by the Navy Navigation Satellite System (rms position accuracy of approximately 60 m). Ice kinematics were determined for periods during which at least three of the four manned camps were providing position data[5].

Omni-directional noise data were collected by eight buoys deployed around the manned camp array during various periods from the spring of 1975 to the spring of 1976. These data were 1/3 octave bands centered at 3.2 Hz, 10 Hz, 32 Hz, and 1000 Hz. The data were 45 s averages sampled every 3 hours. In this paper, we concentrated on the 1000 Hz data. An example of the noise time series for the winter of 1976 (February) is shown in Fig. 1. The data show that the 10 and 32 Hz signals are quite similar. Also, we see energetic, short-term fluctuations in the 1000 Hz data. One feature that was noted at all the AIDJEX acoustic stations during the winter was the period of relatively low noise levels during Julian days 47-57. This corresponds to a time during which no form of ice motion was detected at the manned camps[3]. One will note two anomalous spikes in the 1000 Hz noise record during this period. These spikes are of the order of 20 dB, with some signatures at 10 and 32 Hz. The wind speed at the manned camps had dropped to 1-2 m/s during the first spike. Thus, we classify these noise episodes as anomalous in that they do not correspond to a episode of wind stress or ice motion.

Examples of the time histories of the 1000 Hz and air temperature signals collected during April 1976 are shown in Fig. 2. The 1000 Hz signal shows large (20 dB) fluctuations. These variations are diurnal in period and are apparently related to daily heat fluxes within the ice cover, as seen by the matching air temperature fluctuations. However, note the following. There are numerous instances in which there were air temperature variations but no corresponding noise spikes. Moreover, the noise fluctuations were primarily inversely related to the air temperature changes as opposed to the concept of a 90° phase shift suggested by Milne[4].

Such high frequency anomalies are also seen at other of the AIDJEX acoustic stations. It would appear that thermal microfracturing is a complex function of heat exchange between the ice, air, and water. Fortunately, the AIDJEX data allows us to estimate the heat flux parameters and their time histories.

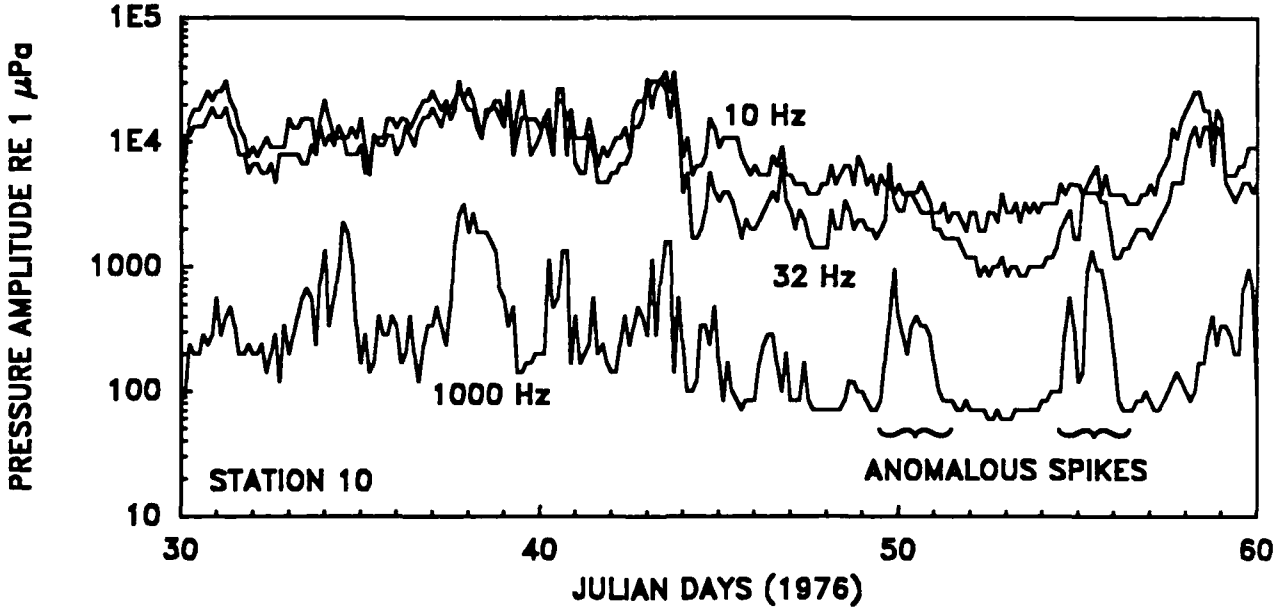

Fig. 1. Ambient noise variations at 10 Hz, 32 Hz, and 1000 Hz at a station in the south-central Beaufort Sea during February 1976.

3. CLASSIFICATION RESULTS

To investigate high frequency noise episodes in the Arctic Ocean, we used the 9 months worth of non-summer acoustic data collected during the AIDJEX study. Noise episodes were defined in two ways: 1) noise variations which had no apparent cause (e.g. ice motion, wind stress) and 2) the lack of noise variations even though there existed strong ice motion or large air temperature changes. The 1000 Hz noise levels were converted from decibels to rms pressure levels re 1 μPa. After documenting all high frequency noise anomalies, we quantified the characteristics of these anomalies in terms of duration, magnitude, and spatial extent. Upon classifying the various anomalies, it was found that the data fell into two categories. The category 1 episodes had greater noise levels (1000-3000 μPa), shorter durations (0.6-1.25 days), and smaller space scales. The category 2 episodes had lower noise levels (<1000 μPa), longer durations (1.75-2.75 days), and larger space scales.

To quantify space scales, we used the times at which a given anomaly was at its strongest intensity at each station. We then calculated the spatial linear gradient S_L of the noise using least squares. Thus, S_L indicates whether the episode was highly local or perhaps

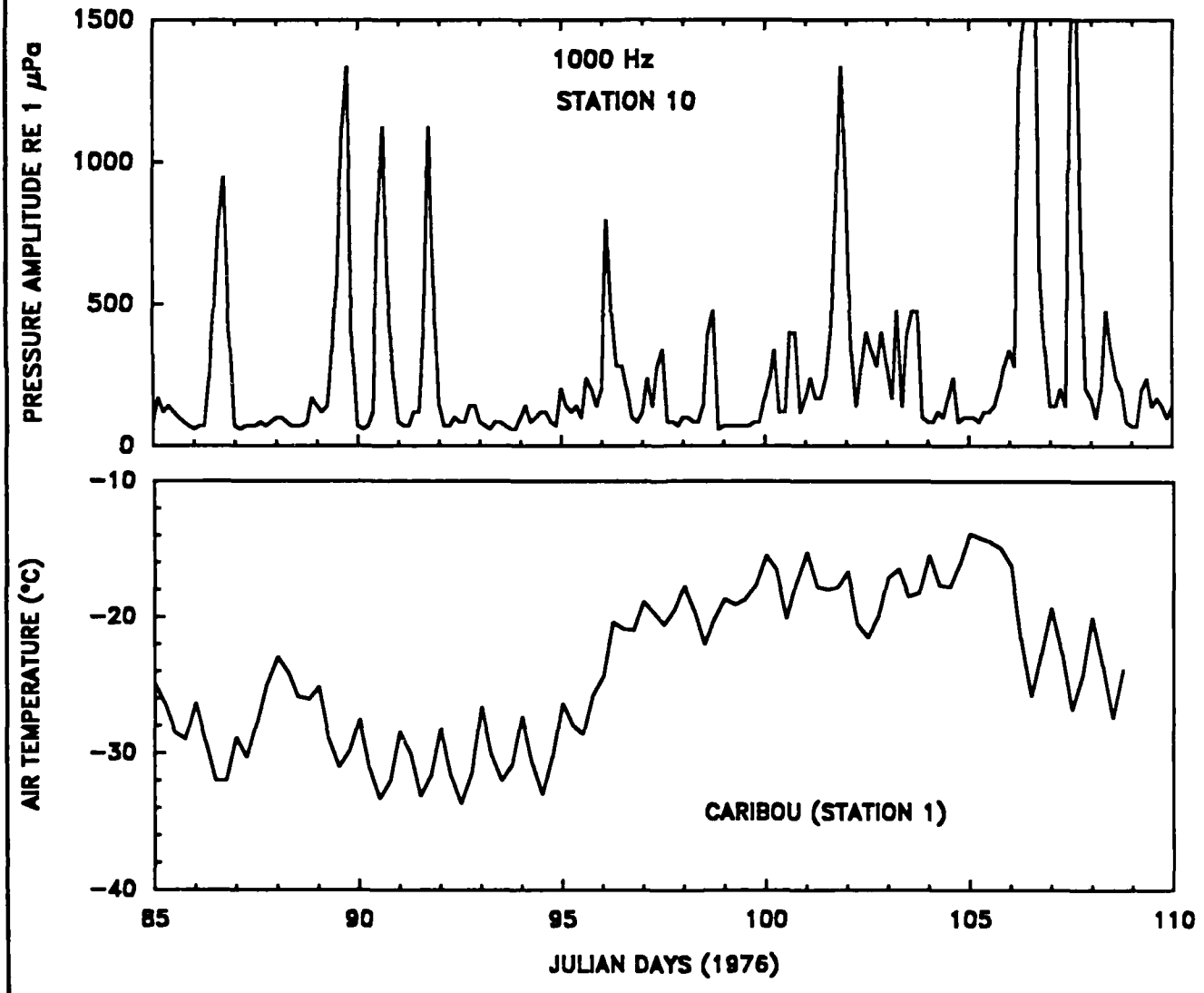

Fig. 2. Fluctuations of 1000 Hz noise and air temperature during late March and April 1976 in the south-central Beaufort Sea.

basin wide. Some examples of the space scale calculations are shown in Fig. 3. Episodes 1 and 3 are of the category 1 type. For these episodes, S_L was of the order of -3 μPa per km. Episode 2 was also a category 1 episode but of a slightly different nature. Here we see that the signature of the episode decreased slowly in one direction (an S_L of -1.5 μPa per km) but decreased much more abruptly in another direction. Episode 2 points out the precipitous regional variations that the category 2 higher frequency noise anomalies can have.

Episode 4 in Fig. 3 is a category 2 anomaly. The actual episode is the first anomalous spike in the 1000 Hz data shown in Fig. 1. Although the noise magnitude was well above the baseline noise level, it was still below 1000 μPa. Also, the presence of the episode was highly directional, occurring primarily within the northwestern and south central Beaufort Sea. In the western and eastern Beaufort, the episode's signature decreased dramatically (e.g., the data points at ~400 km in Fig. 3). Although the magnitudes of the category 2 episodes were less than 1000 μPa, their signatures were more wide spread than the category 1 episodes. Category 2 episodes had S_L values of <-1.0 μPa per km.

There were few category 2 episodes in the data. These all had magnitudes and durations similar to the 1000 Hz noise collected during the summer of 1975. The summer 1000 Hz noise was highly correlated with ice motion[3], implying that the category 2 episodes were also related to ice kinematics. However, this is not always supported by the environmental data, as will be discussed in a later section.

4. NOISE EPISODES AND ENVIRONMENTAL DATA

Examples of category 1 anomalies are shown in Fig. 4 along with additional environmental data. These data are from 10-30 November 1975. In this case, the corresponding ice and wind speed data indicate the 4 significant noise anomalies that are denoted by vertical lines in the noise record. These episodes occurred during the following conditions: small or decreasing wind and/or ice speeds, falling air temperatures, and an increase from lower atmospheric pressure to higher atmospheric pressure. Upon further inspection using data from other stations, we see that these anomalous episodes are precisely what one would expect with the passage of atmospheric frontal systems. The atmospheric lows with their greater winds increase the ice speed. As the low center passes, wind (and ice) speeds decrease on the approach of the following atmospheric high. The circulation between the high and low advects colder air into the region, and the air temperature drops (see Fig. 4).

With the above conditions, there are numerous factors that result in heat loss from the ice. The first of course is sensible heat loss from the ice to the air. But in addition there is a reduction of radiational heat from the atmosphere to the ice. This is a direct result of the drop in the air temperature and the resulting decrease in the black-body radiation of the atmosphere. To confuse matters even more, the colder air normally has less water vapor and smaller percent cloud cover. This reduces the insulating effect of the atmosphere and allows the ice to cool even more.

Another anomalous set of conditions can be found in Fig. 4. These conditions were classified as category 2 episodes and are those occurring during Julian days 316.5-319 and 324-327. Basically, both of these noise episodes occurred while the wind and ice speeds were relatively high. Also, the noise episodes had higher order oscillations superimposed upon them. The episodes were anomalous in that the first episode had a baseline magnitude of nearly 800 μPa while the second had a baseline magnitude of ~400 μPa. This seems surprising since the ice speed maximum during the first noise episode was almost half that during the second noise episode. A review of all the ice kinematic data showed that the field of ice before and during the first noise episode had undergone a net convergence. However, at the beginning of the second noise episode, the field of ice underwent a net divergence. This is an instance in which the concentration of the ice field greatly affects microfracturing. Lewis and Denner[3] had shown that ice speed was positively correlated with higher frequency noise but ice divergence was negatively correlated with the approach of winter. Since divergence is the fractional rate of area change, the results imply greater noise while the ice field is compacting. Thus, the additional noise magnitudes during the first episode would be a result of the crushing of new ice in leads and/or the

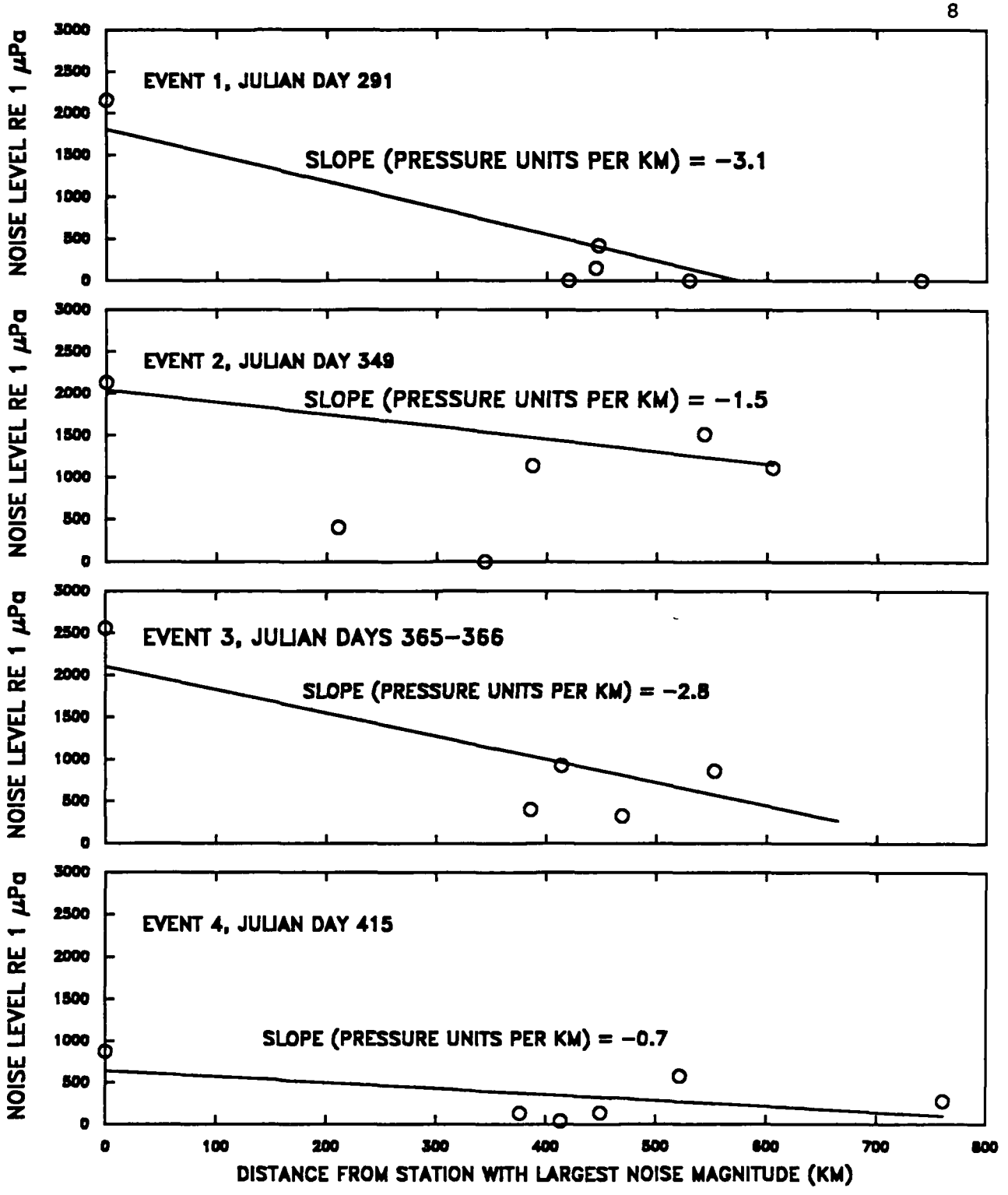

Fig. 3. Spatial variations of maximum 1000 Hz noise levels for four episodes in the Beaufort Sea during 1975 and 1976.

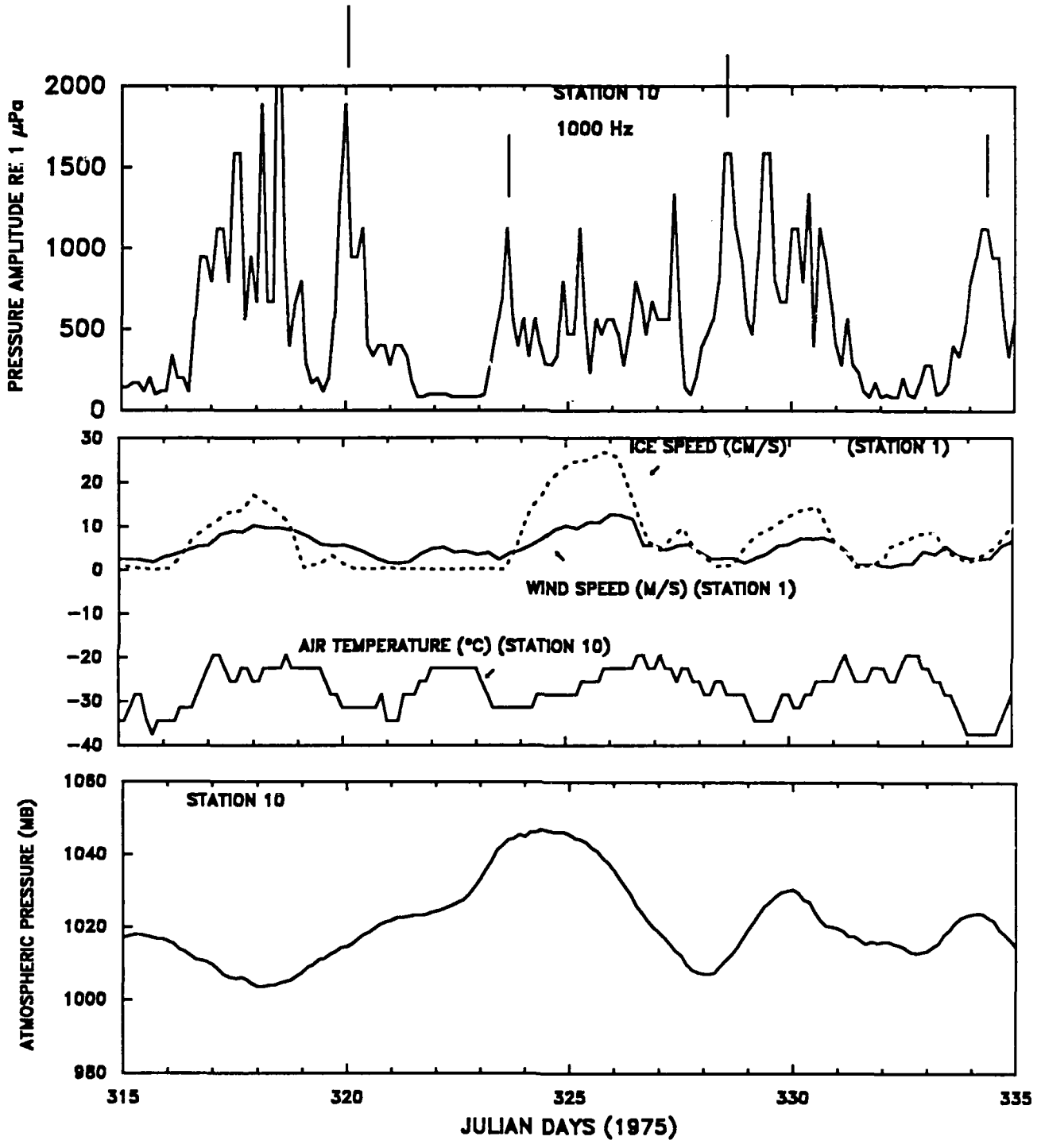

Fig. 4. Time histories of 1000 Hz under-ice noise (top), ice speed, wind speed, and air temperature (center), and atmospheric pressure (bottom) in the central Beaufort Sea during November 1975. The vertical lines (top figure) denote times during which the 1000 Hz noise was, at most, weakly associated with ice kinematics and wind forcing.

increased floe-floe interaction occurring as the ice field compacted.

A second set of higher frequency noise anomalies can be picked out in the spring data shown in Fig. 2. Once again, these are category 1 noise episodes, or non-events as the case may be. These data begin on 26 March 1976. We see occasional daily noise spikes along with rather regular daily air temperature fluctuations. The correspondence between daily air temperature and noise fluctuations was first pointed out by Milne[4] and has been associated with thermal microfracturing due to heat loss from the ice to the air. Moreover, the noise maximums have been assumed to occur when the air temperature was dropping at its maximum rate (i.e., the point at which the cooling of the top layer of ice would be greatest). However, Fig. 2 points out numerous instances in which there exists significant air temperature fluctuations but no noise spikes. In addition, a blowup of the data from Julian days 88-92 (Fig. 5) shows that the noise maximums tended to occur from 6 to 9 a.m. local time while the maximum drops in air temperature occurred at about 6 p.m. local time. Clearly, there are pertinent factors that we have yet to consider.

In all the environmental data that we have considered, the spring-time daily noise spikes have some common characteristics. They all tended to occur during periods of relatively high atmospheric pressure and low atmospheric inversion heights. The implication is that they tend to occur during cloud-free conditions, and this supposition is supported by the meteorological observations taken at the manned camps. The presence or absence of cloud cover primarily affects longwave radiation from the atmosphere to the ice. Daily heating of the ice by spring-time solar radiation can be maintained by such a cloud cover at night, and little thermal microfracturing occurs even though the air temperature may drop.

Such a mechanism provides a reasonable explanation for the variations in daily higher frequency noise spikes. However, the meteorological observations indicate a number of times during which the sky was clear but no 1000 Hz noise spike occurred. During such occurrences, the observers noted factors such as ice fog and blowing snow. These phenomena must also affect heat balances within the ice, again in terms of radiational heat flux.

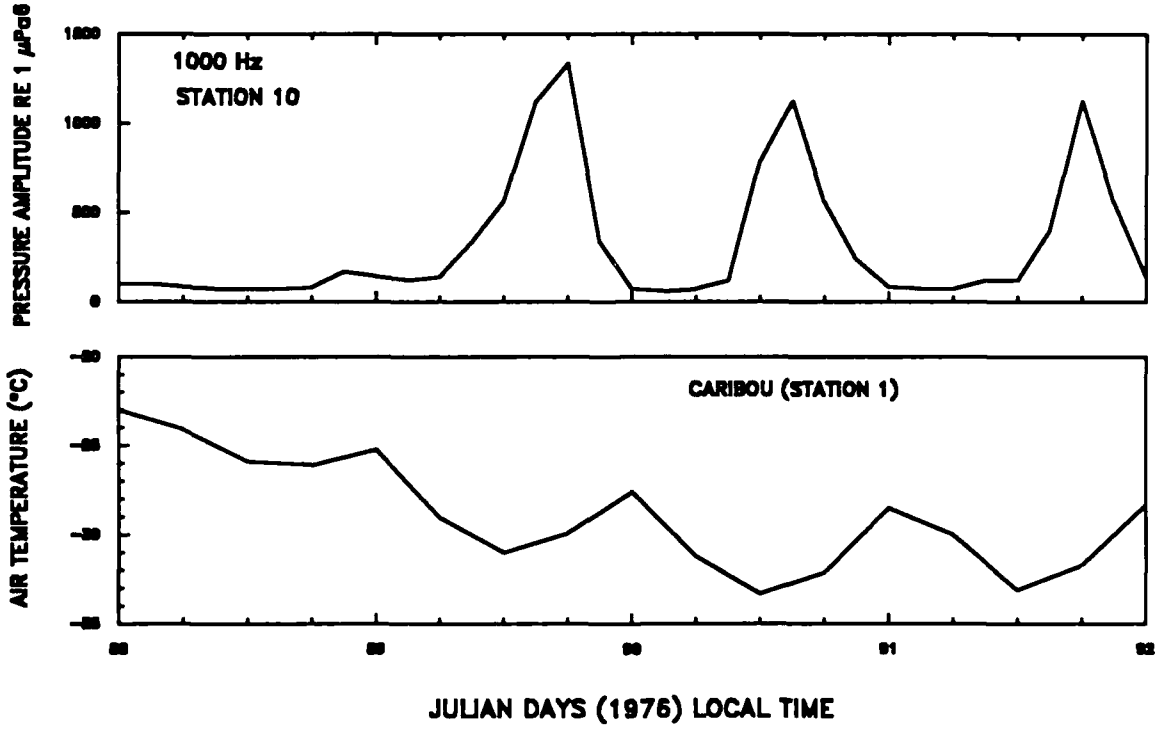

Fig. 5. Corresponding fluctuations of 1000 Hz noise and air temperature for a four day period in early April 1976.

5. HEAT FLUX IN SEA ICE

The vertical flux of heat within sea ice may be written as

$$\rho_I \, c_I \, (dT/dt) = d(k_I \, dT/dz)dz \qquad (1)$$

where ρ_I is the ice density (917 kg/m^3), c_I is the specific heat of ice (a function of temperature and salinity), T is the ice temperature, t is time, z is positive upwards from the ice surface, and k_I is the thermal conductivity of ice (2.03 W m^{-1} °C^{-1}). Assume that we have surface temperature fluctuations, the magnitude of which decays exponentially with the depth of the ice. If ρ_I, c_I, and k_I were constant within the ice, then the solution to (1) is

$$T = (T_s - T_b)\, z/H + T_s + \\ + T_s' \, e^{\alpha z} \cos(ft + \alpha z) \qquad (2)$$

where T_s is the mean surface temperature, T_b is the mean temperature at the ice bottom, H is the ice thickness, T_s' is the amplitude of the surface temperature fluctuations, f is the frequency of the temperature fluctuations, and α^{-1} is the e-folding depth of the temperature fluctuations with

$$\alpha = (\rho_I \, c_I \, f/2 \, k_I)^{1/2}.$$

In this case, the thermal signal travels through the ice as a damped sinusoid. For a daily period and typical values of ρ_I, c_I, and k_I, α^{-1} is of the order of 20 cm. Thus, most of the microfracturing of sea ice can be expected to occur within the top 30 cm of the ice for a diurnal heating cycle. In this case, one would expect arctic ambient noise generated by thermal microfracturing to coincide closely with the drop in temperature of the ice surface. As the frequency f becomes smaller (as with fluctuations associated with atmospheric fronts), α^{-1} becomes large. With these conditions, our expression shows that the ice temperatures at various depths would fluctuate in near unison, with the vertical gradient of temperature being close to linear.

There are several problems with the above analytical solution when applied to heat in sea ice. First, the specific heat of sea ice increases by an order of magnitude from the surface to about 2-3 m. This is because of the warmer and saltier ice at the bottom. Secondly, thermal conductivity can vary considerably with temperature and salinity. Thus, to consider such variations, one is required to numerically model heat flux in sea ice. If the ice is divided into n layers, (1) can be approximated in finite difference form as

$$H_n \; \rho_I \, c_I \, (dT/dt) \qquad (3)$$
$$= 2 \, (k_{I,n+1}(T_{n+1} - T_n)/(H_{n+1} + H_n) - \\ - k_{I,n}(T_n - T_{n-1})/(H_n + H_{n-1}))$$

where n is the layer number (increasing upwards), T represents the average temperature of the n^{th} layer, $k_{I,n}$ is the thermal conductivity at the bottom of the n^{th} layer, and H_n is the thickness of the n^{th} layer. For the bottom layer of the ice, a temperature of -2 °C is typical of arctic ice conditions, a result of the temperature of the underlying ocean water. Thus, the conductive heat flux from the ocean in the bottom layer n = b modifies (3) such that

$$H_b \; \rho_I \, c_I \, (dT/dt) \qquad (4)$$
$$= 2 \, (k_{I,b+1}(T_{b+1} - T_b)/(H_{b+1} + H_b) - \\ - k_{I,b}(T_b + 2°)/H_b)$$

In the top layer of ice, there exist heat exchanges at the ice surface that include sensible and evaporative heat fluxes (QSENS and QEVAP), short wave solar radiation (QSLR), longwave radiation from the ice to the atmosphere (QBI), and longwave back radiation from the atmosphere (QBA). Thus, for the top layer n = t, (3) becomes

$$H_t \; \rho_I \, c_I \, (dT/dt) = \qquad (5)$$
$$QSLR + QSENS + QEVAP + QBI + \\ + QBA - 2 \, k_{I,t}(T_t - T_{t-1})/ \\ /(H_t + H_{t-1})).$$

The above expression accounts for the flux of heat from the underlying layer of ice and from the ice surface. The above expression is also used to calculate a near-surface temperature to be used in determining sensible and radiational heat flux terms.

The unknowns in our model are the ice temperatures and the Q terms. We parameterize the Q terms in the following manner:

QSLR - is specified as a function of local time based on incoming radiation QSOLAR and albedo ALB measured at the ice surface, (1.0 - ALB) QSOLAR. During the AIDJEX experiment, an extensive amount of data was collected for these variables[6]. For typical spring conditions, approximately 400 W/m^2 was measured as a maximum for QSOLAR and occurred at local noon. The sun was below the horizon from ~2000 to ~0400 hours local, and QSOLAR was zero for those times. Albedos averaged 0.8. For fall conditions (November), the sun was below the horizon for most of the day, and QSOLAR was negligible.

QSENS - using the air temperature T_a along with T_t, the sensible heat flux is parameterized by[7]

$$QSENS = \rho_a C_p C_s U (T_a - T_t)$$

where ρ_a is the air density (~1.395 kg/m^3 for air temperatures of about -20 °C), C_p is the specific heat of air (10^3 W s/kg °C for cold air), U is the wind speed (m/s), and C_s is a bulk transfer coefficient (1.2×10^{-3}). Based on the AIDJEX air temperature data, we specify T_a as a function of time for this model.

QEVAP - is considered negligible. Maykut[7] compared a number of observations and found QEVAP to be considerably smaller than QSENS during spring and fall. Thus, for our purposes, we ignore this term.

QBI - is specified directly as a function of the surface temperature T_s of the ice using

$$QBI = e_L \sigma (273.16 + T_t)^4$$

where e_L is the effective emissivity for ice (0.97) and σ is the Stefan-Boltzmann constant (5.67×10^{-8} $W/m^2 °K$).

QBA - is specified directly as a function of the air temperature T_a and the fractional cloud coverage C using[8]

$$QBA = e^* \sigma (273.16 + T_a)^4$$

where e^* is the effective emissivity of the atmosphere. Since the increase in atmospheric moisture associated with greater cloud coverage results in an increase in e^*, we specify C in the model and use

$$e^* = 0.7855 (1 + 0.2232 C^{2.75}).$$

Thus, equations (3) - (5) give us n equations in n unknowns for n levels within the ice. Using our analytical solution as a standard, the numerical model was validated and tested with a 15 cm vertical grid spacing. To simulate conditions in the Beaufort Sea, we let the ice thickness be 2.4 m. Based on the work of Schwarz and Weeks[9], the temperature at the bottom of the ice was held at -2 °C while the salinity of the ice was allowed to vary from 0°/oo at the surface to 3°/oo at the bottom. The coefficient of thermal conductivity was expressed as a function of the salinity and temperature between two ice layers using[10]

$$k_I = (2.03 + Sx107.43/(T - 273.16)) \text{ W } m^{-1} \text{ } °K^{-1}.$$

where S is the ice salinity in ppt. Thus, the thermal conductivity was allowed to change as the thermal wave passed through the ice. Finally, the changes of the specific heat of ice were approximated in a linear fashion in each ice layer given the salinity of the layer[11]. Maximum changes of the specific heat would occur in the lower ice layers. For a salinity of 2°/oo, one could have a value of 2.66 cal/g °C at -2 °C but only 0.48 cal/g °C at -22 °C. However, the bottom boundary condition of a constant -2 °C resulted in relatively warm temperatures in the bottom 4 or 5 layers of the ice. Thus, the specific heat in the bottom ice layers tended toward larger values.

A number of simulations were run until equilibrium conditions were obtained within the ice layers. Equilibrium implies that the ice temperature in each layer at a particular time in the cycle of surface conditions (solar radiation, air temperature, etc.) was identical to that of the previous cycle of surface conditions. At each time step, dT/dt was calculated for each layer. We then integrated under the curve of negative dT/dt's versus z:

$$F = \int dT/dt \, dz \quad \text{for } dT/dt < 0.$$

Thus, F is our estimator of the total ice undergoing tensile stress and serves as a proxy for the net thermal microfracturing of the ice.

SPRING SIMULATION RESULTS

One set of simulations was run with an ice albedo of 0.8, spring-time solar radiation (maximum of 400 W/m² at 1200 hrs), a daily air temperature cycle of frequency ω (maximum temperature at 1500 hrs), and very light winds (0.1 m/s). In these calculations, the sensible heat flux was negligible and the primary balances were between the incoming solar radiation and outgoing back radiation. The simulations and their results (Table 1) are as follows:

1) $T_a = (-30 + 3.5 \cos \omega t)$°C and C = 0 - These are similar to cold, spring-like conditions under a high pressure system (no clouds). The maximum in F (largest negative value) was -2.3 10^{-5} °C m/sec and occurred at 1900 hrs local. Thus, as the sun dropped low on the horizon, the ice cooled rapidly by longwave back radiation. Moreover, the simulation showed that there was an accumulation of heat in the top-most ice layer which drove a thermal wave downward into the second ice layer from 1300-1500 hrs. The maximum cooling that occurred at 1900 hrs was a product of net radiative heat loss at the ice surface.

2) $T_a = (-15 + 3.5 \cos \omega t)$°C and C = 0 - These are conditions similar to warmer spring periods without cloud cover. The results are identical to those above. It is obvious that our tensile stress parameter F is only partially successful as a predictor of microfracturing. With the warmer conditions, the resulting warmer ice will be less rigid and would fracture less. This implies a refinement for future modeling through the incorporation of the mechanics of the ice (e.g., the thermal coefficient of expansion and the expansion modulus, both functions of temperature).

3) $T_a = (-15 + 3.5 \cos \omega t)$°C and C = 0.8 - The model was allowed to run until equilibrium under these relatively warm, cloudy conditions. The final 24 hrs of the simulation were then run with C = 0. This run was to consider the heat fluxes as the clouds over the ice dissipate and the net longwave radiation away from the ice increases the following day.

Equilibrium Conditions	Most Negative F	Time of F Maximum
Experiment 1:		
$T_a = (-30 + 3.5 \cos lt)$°C	-2.3 10^{-5}	1900
Percent Cloud Cover = 0%		
Experiment 2:		
$T_a = (-15 + 3.5 \cos lt)$°C	-2.2 10^{-5}	1900
Percent Cloud Cover = 0%		
Experiment 3:		
$T_a = (-15 + 3.5 \cos lt)$°C	-2.5 10^{-5}	0100
Percent Cloud Cover = 80%;	-2.4 10^{-5}	1900
Last 24 hrs		
Percent Cloud Cover = 0%		
Experiment 4:		
$T_a = (-15 + 3.5 \cos lt)$°C	-5.5 10^{-5}	0100
Percent Cloud Cover = 80%	-3.1 10^{-5}	1900
For Last 24 hrs,		
$T_a = (-30 + 3.5 \cos lt)$°C		
Percent Cloud Cover = 0%		

Table 1. Results of numerical simulations for sea ice that is 2.4 m thick and has no snow cover. Parameters are albedo = 0.8, QSOLAR maximum = 400 W/m² at 1200 hrs, U = 0.1 m/s, and daily oscillations of T_a with the maximum at 1500 hrs. The thermal microfracturing parameter F has the units of °C m/sec.

In such a situation, there was a double maximum in F for the last 24 hours; $-2.5\ 10^{-5}$ °C m/sec at 0100 local and $-2.4\ 10^{-5}$ °C m/sec at 1900 hours local. The maximum at 0100 hrs was the result of the abrupt removal of the insulating effect of the cloud cover in that time step (0000 to 0100 hrs local). The second maximum is the result of the cooling of the first 15 cm of ice by radiation.

4) $T_a = (-15 + 3.5 \cos\ \omega t)$ °C and C = 0.8 - Again, the model was allowed to run to equilibrium under the above conditions (warmer air, cloudy skies). During the last 24 hours, however, the conditions were $T_a = (-30 + 3.5 \cos\ \omega t)$ °C and C = 0. Thus, this is quite similar to the passage of a cold front in which cold air is advected into the region and the cloud cover dissipates. Again, there was a double maximum in F; $-5.5\ 10^{-5}$ °C m/sec at 0100 hrs local time and $-3.1\ 10^{-5}$ °C m/sec at 1900 local. Along with the removal of the cloud cover (see the previous simulation), the drop in the air temperature resulted in less longwave radiation (heating) from the sky to the ice. Thus, the maximum in F at 0100 local was still a phenomena related to atmospheric longwave radiation, with the rapid drop in air temperature having a slightly greater effect than the dissipation of the cloud cover. Due to the light winds (0.1 m/s), the sensible heat flux was still of no consequence.

The above spring-time simulations indicate the importance of the radiational heat balance. The maximum net lowering of the temperature in the top ice layer that always occurred at 1900 hrs would imply maximums in thermal microfracturing during spring evenings. As wind speed is increased in the model, the time of the maximum in F remains the same (1900 hrs), but the magnitude decreases slightly. This is a result of the additional heat loss throughout the rest of the day by sensible heat flux.

Spring Simulations with a Snow Cover

Although our simulations have been enlightening, there were no model runs that would explain a maximum in the decrease of ice temperature at 0600 hrs as implied by the noise data (Fig. 5). One of the principle components missing in our model is snow cover. The average snow thickness on the central arctic ice

Equilibrium Conditions	Most Negative F	Time of F Maximum	Snow Cover
Experiment 1:			
$T_a = (-30 + 3.5 \cos$ lt)°C	$-0.4\ 10^{-5}$	0400	15 cm
Percent Cloud Cover = 0%	$-0.1\ 10^{-5}$	0600	30 cm
Experiment 2:			
$T_a = (-15 + 3.5 \cos$ lt)°C	$-0.3\ 10^{-5}$	0300-0400	15 cm
Percent Cloud Cover = 0%	$-0.1\ 10^{-5}$	0600	30 cm
Experiment 3:			
$T_a = (-15 + 3.5 \cos$ lt)°C	$-0.4\ 10^{-5}$	0400	15 cm
Percent Cloud Cover = 80%;	$-0.4\ 10^{-5}$	2000	15 cm
For Last 24 hrs	$-0.1\ 10^{-5}$	0600-0700	30 cm
Percent Cloud Cover = 0%	$-0.1\ 10^{-5}$	2400	30 cm
Experiment 4:			
$T_a = (-15 + 3.5 \cos$ lt)°C	$-0.8\ 10^{-5}$	0400	15 cm
Percent Cloud Cover = 80%;	$-0.7\ 10^{-5}$	2400	15 cm
For Last 24 hrs,	$-0.2\ 10^{-5}$	0800	30 cm
$T_a = (-30 + 3.5 \cos$ lt)°C	$-0.3\ 10^{-5}$	2400	30 cm
Percent Cloud Cover = 0%			

Table 2. Results of numerical simulations for sea ice that is 2.4 m thick, the top 15 or 30 cm being snow. Parameters are albedo = 0.8, QSOLAR maximum = 400 W/m² at 1200 hrs, U = 0.1 m/s, and daily oscillations of T_a with the maximum at 1500 hrs. The thermal microfracturing parameter F has the units of °C m/sec.

pack varies from about 5 cm in August to ~40 cm in May. The heat storage capacity of snow is about a third that of ice, but ice conducts heat about six times more rapidly than snow. Thus, snow will act to damp out and phase shift the surface heating and cooling signals that give rise to the thermal wave within the ice.

To consider the effects of snow cover on the ice, we performed the above simulations with the first one or two layers of the model being snow. The conductive heat fluxes on each side of the snow/ice interface were made equal by calculating an appropriate interfacial temperature. This interfacial temperature was then used in the next time step for calculating heat fluxes in the snow above the interface and in the ice below the interface. The simulations and their results (Table 2) are as follows:

1) $T_a = (-30 + 3.5 \cos \omega t)°C$ and C = 0 - (cold spring-like conditions, no clouds). The largest negative value of F was -0.4 10^{-5} °C m/sec and occurred at 0400 hrs local time for a 15 cm layer of snow. With 30 cm of snow cover, this dropped to -0.1 10^{-5} °C m/sec at 0600 hrs.

2) $T_a = (-15 + 3.5 \cos \omega t)°C$ and C = 0 - (warmer spring periods without cloud cover). For a 15 cm cover of snow, the maximum in F was -0.3 10^{-5} °C m/sec at 0300-0400 hrs, about 25% less than colder conditions above. With 30 cm of snow, this changed to -0.1 10^{-5} °C m/sec at 0600 hrs.

3) $T_a = (-15 + 3.5 \cos \omega t)°C$ and C = 0.8 - (warmer, cloudy conditions). The final 24 hrs of this simulation was run with C = 0. There was a double maximum in F for the last 24 hours for both a 15 cm and a 30 cm snow cover. For the 15 cm snow cover, F was -0.4 10^{-5} °C m/sec at 0400 hrs and was still increasing when it reached -0.4 10^{-5} °C m/sec at 2400 hrs. For the 30 cm snow cover, F was -0.1 10^{-5} °C m/sec at 0600-0700 hrs and reached -0.1 10^{-5} °C m/sec at 2400 hrs.

4) $T_a = (-15 + 3.5 \cos \omega t)°C$ and C = 0.8 - (warmer air, cloudy skies). During the last 24 hours, the conditions were $T_a = (-30 + 3.5 \cos \omega t)°C$ and C = 0. For 15 cm of snow, F had two maximums: -0.8 10^{-5} °C m/sec at 0400 hrs and -0.7 10^{-5} °C m/sec at 2400 hrs. For 30 cm of snow cover, F had a maximum of -0.2 10^{-5} °C m/sec at 0800 hrs and then another of -0.3 10^{-5} °C m/sec at 2400 hrs.

Snow cover has now changed the entire complexion of our predicted thermal microfracturing. The maximums in F have been reduced substantially. In addition, the snow cover has shifted the times of the maximums of F from 1900 hrs to between 0300 hrs (15 cm of snow) to 0800 hrs (30 cm of snow). This is precisely the time frame at which we have seen under-ice noise maximums in the data from the arctic.

Finally, we make a comment on the nature of the maximums in F in the presence of snow cover. Without snow, F has maximums at the times of drops in net radiation at the surface of the ice, 0100 and 1900 hrs. This occurs in the top 15 cm of ice. With snow cover, there is never a surplus of heat in the top ice layer which would conduct heat downward. The conduction of heat is always upward from the ocean, through the ice, and into the overlying snow. Thus, the thermal microfracturing for sea ice with a snow cover is entirely a process of the loss of heat upward toward the atmosphere. This occurs over the top 45 cm of ice.

Fall Simulations

A number of runs were made under fall conditions in which one would expect less snow cover and no solar heating. These simulations were made with cloud cover C = 0. The following (Table 3) are the results:

1) T_a = -15°C, U = 0.1 m/s - After reaching equilibrium conditions, the air temperature was set to -30°C for the last 24 hrs. This is similar to a cold front moving in with light winds. The maximum in F was -3.1 10^{-5} °C m/sec at 0100 hrs local. Thus, the loss of heat from atmospheric longwave radiation resulted in a heat loss from the ice surface layer as soon as the air temperature dropped.

2) T_a = -15°C, U = 5 m/s - These initial conditions are similar to those preceding a low pressure system. Winds were brisk and air temperatures were relatively warm. After equilibrium, the last 24 hours were run with T_a = -30°C and U = 0.1 m/s (similar to conditions after the passage of an atmospheric frontal system). Once again, the maximum in F

occurred at 0100 hrs and was -4.7 10^{-5}° C m/sec. This larger F was a result of warmer ice conditions when compared to the previous simulation. The stronger winds and the initial -15° C air temperature resulted in the ice surface layers being about -20° C. In the previous simulation under light winds, the equilibrium ice surface temperature was only -24.7° C. Thus, this simulation had a larger radiational heat flux from the ice to the air, and the larger F value reflects this fact.

3) T_a = -15° C, U = 0.1 m/s, 15 cm of snow - Since one would expect less snow in the fall, we made this simulation with only one 15 cm layer of snow. After reaching equilibrium, the air temperature was set to -30° C for the following 24 hrs. This run gave a maximum F value of -0.4 10^{-5}° C m/sec at 0900-1000 hrs. The snow cover had cooled quite rapidly and pulled heat from the three surface layers of the ice.

6. SIMULATION OF JULIAN DAYS 90-110, 1976

The data collected during the AIDJEX study allows one to simulate under-ice noise variations using the heat flux model. We consider the April 1976 time frame shown in Fig. 6. This figure shows a number of 1000 Hz noise spikes which we wish to model using the ice fracturing variable F. Of the five major spikes seen in the data, only the one which occurred on Julian days 95-96 was associated with ice motion.

To force the thermal model, we used environmental data collected 70-100 km north of the noise station in the Beaufort Se- The observed wind speed and air temperature data are shown in Fig. 7. A distinct warming trend is seen to have begun on day 95. Daily air temperature variations can be seen throughout the period, with a major drop occurring on day 105.

Solar radiation was also measured, and the daily variations can be seen in Fig. 8. There tended to be somewhat of a reduction in radiation during Julian days 91-94 and again during days 95-98. The albedo was also measured at the AIDJEX manned camps, and the average is shown in Fig. 9. These data show that the albedo tended to decrease during the period to be simulated.

Also shown in Fig. 9 is the percent of cloud cover. This variable was estimated from the AIDJEX meteorological observations of cloud height, type, and approximate coverage. Such an estimate (to determine back radiation from the atmosphere) is difficult to make and rather subjective. Thus, cloud cover is the variable in which we have the least amount of confidence for the heat flux simulation. The data suggest that the skies were relatively clear at the beginning and end of the simulation

Equilibrium Conditions	Most Negative F	Time of F Maximum	Snow Cover
Experiment 1:			
T_a = -15° C, U = 0.1 m/s; For Last 24 hrs, T_a = -30° C	-3.1 10^{-5}	0100	0 cm
Experiment 2:			
T_a = -15° C, U = 5 m/s; For Last 24 hrs, T_a = -30° C, U = 0.1 m/s	-4.7 10^{-5}	0100	0 cm
Experiment 3:			
T_a = -15° C, U = 0.1 m/s; For Last 24 hrs, T_a = -30° C	-0.4 10^{-5}	0900-1000	15 cm

Table 3. Results of numerical simulations for sea ice that is 2.4 m thick, with or without a snow cover. Parameters are QSOLAR = 0 W/m², no daily oscillations of T_a, and cloud cover is zero. The thermal microfracturing parameter F has the units of °C m/sec.

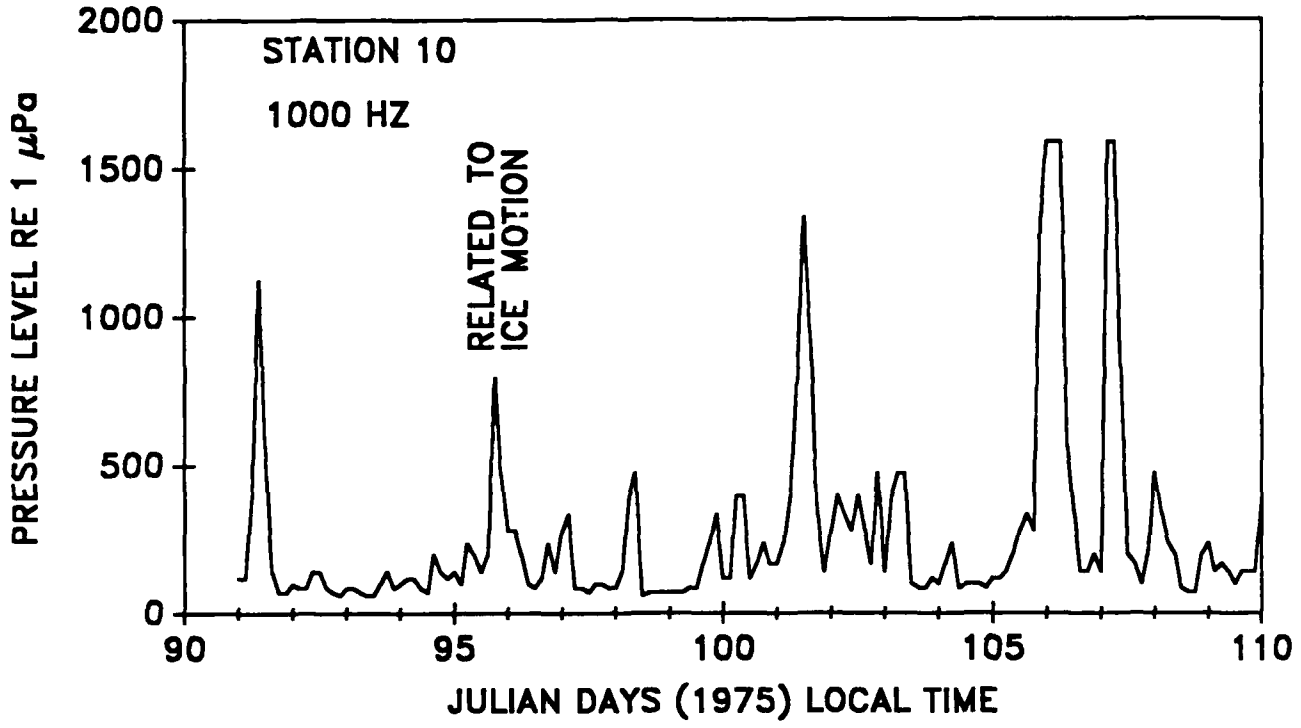

Fig. 6. Observed 1000 Hz noise in the south central Beaufort Sea during April 1976.

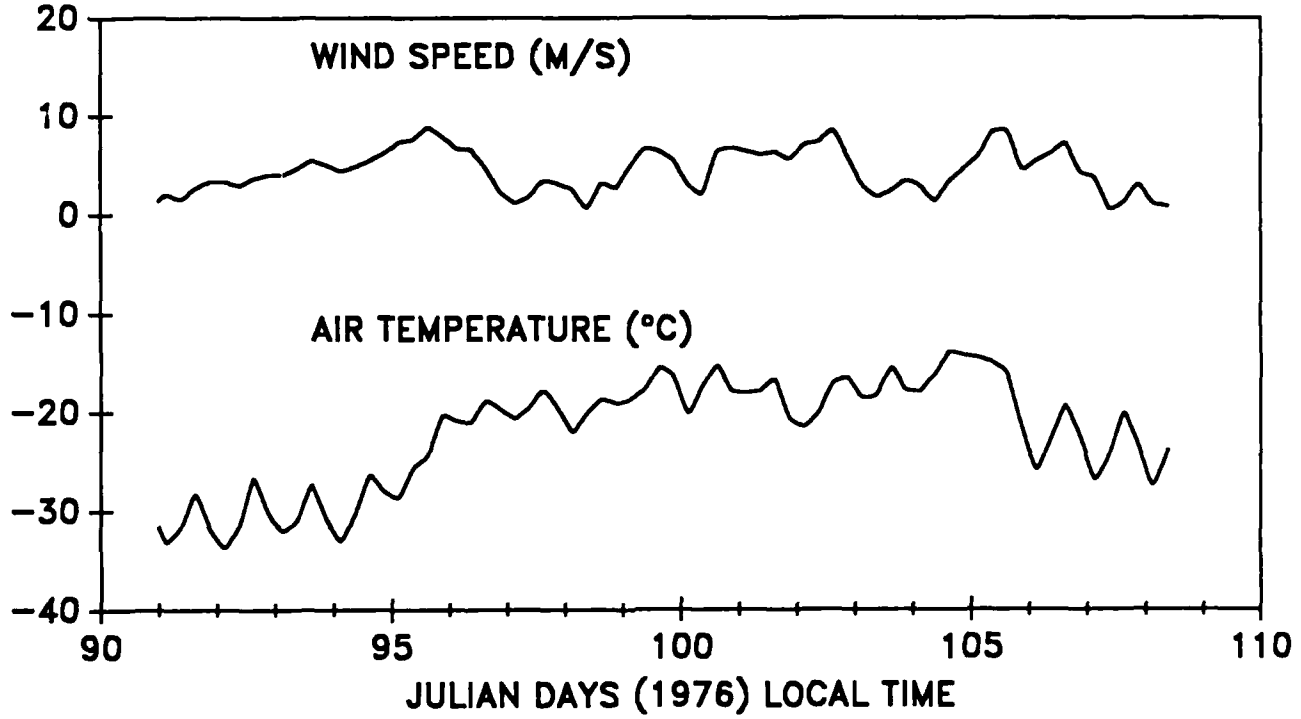

Fig. 7. Observed 10 m wind speed and air temperature variations in the central Beaufort Sea during April 1976.

period. Between Julian days 95 and 105, the estimated cloud cover was highly variable and oscillated between 0.4 and 1.0.

The heat flux model was run for 120 one hour time steps using the initial values of all the environmental parameters. This allowed the ice temperatures to reach a near equilibrium between the environment, the underlying ocean water (at -2.0°C), and the snow cover. Two simulations were made. The first had a 15 cm layer of snow, and these results are shown in Fig. 10a. We plotted -F so that an easy comparison could be made with the observed noise variations in Fig. 6. The values of -F show distinct spikes at the beginning and end of the simulation period. However, the particular -F spikes on Julian days 92-94 and 108 are not seen in the 1000 Hz noise data. We also note that the 1000 Hz noise spike on Julian day 101 corresponds to a -F spike occurring ~12 hrs later.

The second simulation used a snow cover of 30 cm. The results (Fig. 10b) still show the -F spikes during days 91-94 and 106-108. In addition, the -F spike which corresponds to the 1000 Hz noise spike of day 101 still exists but is now phased lagged by ~15 hrs.

Considering that these simulations used environmental data collected some 70-100 km distance from the noise station, the agreement between the modeled fracturing and the observed noise is excellent. We still must account for the fact that the model produced spikes while the 1000 Hz noise had none (days 92-94 and 108). There is the possibility that cloud cover at the noise collection station was quite different than that at the stations where the rest of the environmental data were collected. However, the meteorological observations point out other variables which could be a factor in insulating the pack ice. As previously noted, there were observations of blowing snow and ice fog during days 92-94. It is not unreasonable to assume that such phenomena affects the transmission of radiational heat. Two possibilities exist. The first is that the blowing snow and ice fog could substantially reduce the solar radiation reaching the surface of the pack ice. Thus, the ice is prevented from going through its diurnal warming phase. The second possibility is that the blowing snow and ice fog act as an insulator and prevents radiational cooling at the surface of the pack ice. This would prevent the ice from undergoing the daily cooling phase.

7. DISCUSSION

As previously mentioned, higher frequency noise can have very short length scales during the fall (~150 km), and these increase to only 300 km during spring. For 32 Hz arctic ambient noise, length scales for the same periods of time are 660 km (fall) and 1000 km (spring)[2]. Although higher frequency noise appears to be dominated by thermal microfracturing for the non-summer months (as opposed to motion-induced microfracturing), the atmospheric driving would still imply longer length scales. This is supported by the length scales of the AIDJEX air temperature data, which are on the order of 370 km for fall and winter and 1000 km for spring. But our modeling has shown that snow cover can greatly modify the response of the ice to atmospherically-induced microfracturing. Snow thickness is a parameter that can have a large variance in its spatial distribution. During fall, the arctic ice pack receives its first new blanketing of snow as various fronts move through the arctic. It is at this time that one would expect the most uneven spatial distribution of snow cover. As a result, atmospherically-induced thermal microfracturing in the ice also can be expected to be unevenly distributed in space. Hence we have the short space scales of higher frequency noise during fall (see Episode 1, Fig. 3). As winter continues, the spatial distribution of snow cover would become more even. Thus, the increase of space scales from fall to spring is more likely a result of a more evenly distributed snow cover than a greater compactness and rigidity of the ice field. However, the winter and spring space scales are still relatively short (Fig. 3). It would appear that snow cover (and perhaps cloud cover) is still modifying the response of ice to thermal microfracturing. This is quite possible since the average snow cover in May is only 40 cm. Arctic winds tend to strip snow from flatter regions and deposit it around ridges and hummocks on the ice pack. Thus, the winter and spring higher frequency noise can still be expected to have space scales shorter than the atmospheric forcing. A striking example of this is shown by Lewis and Denner[3] (their figures 13-16).

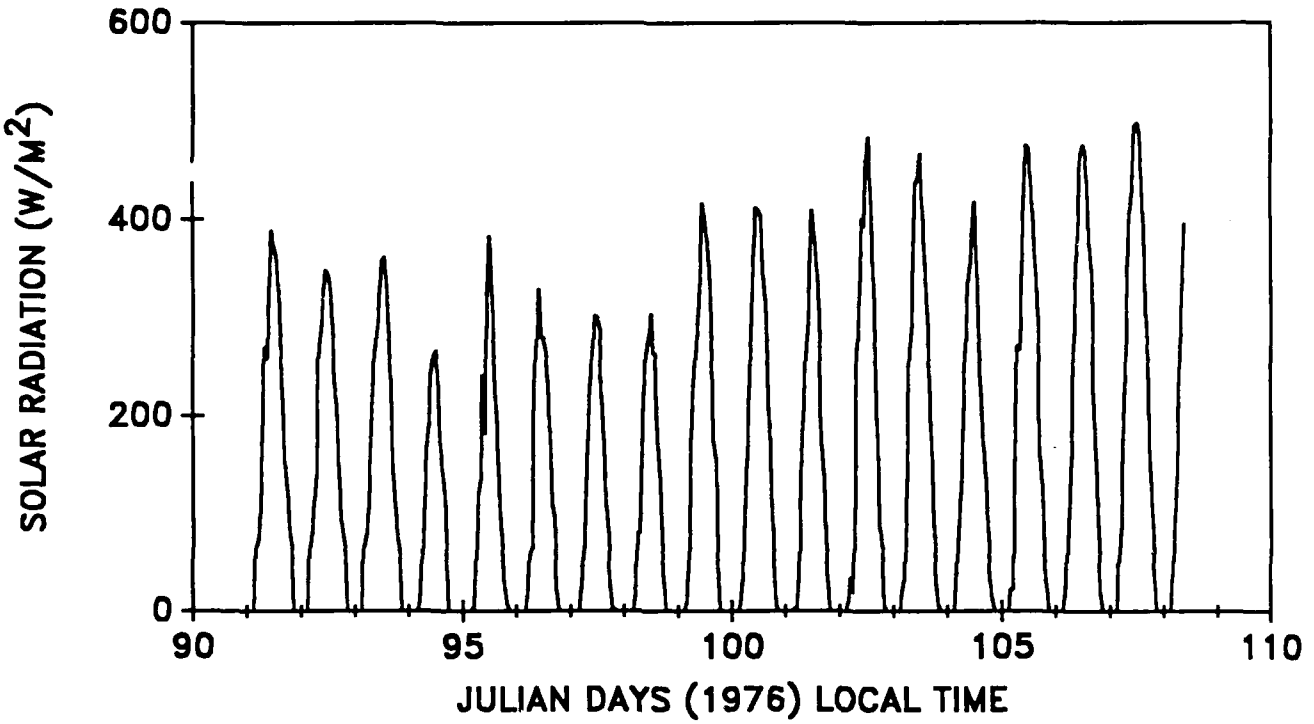

Fig. 8. Observed incoming solar (shortwave) radiation in the central Beaufort Sea during April 1976.

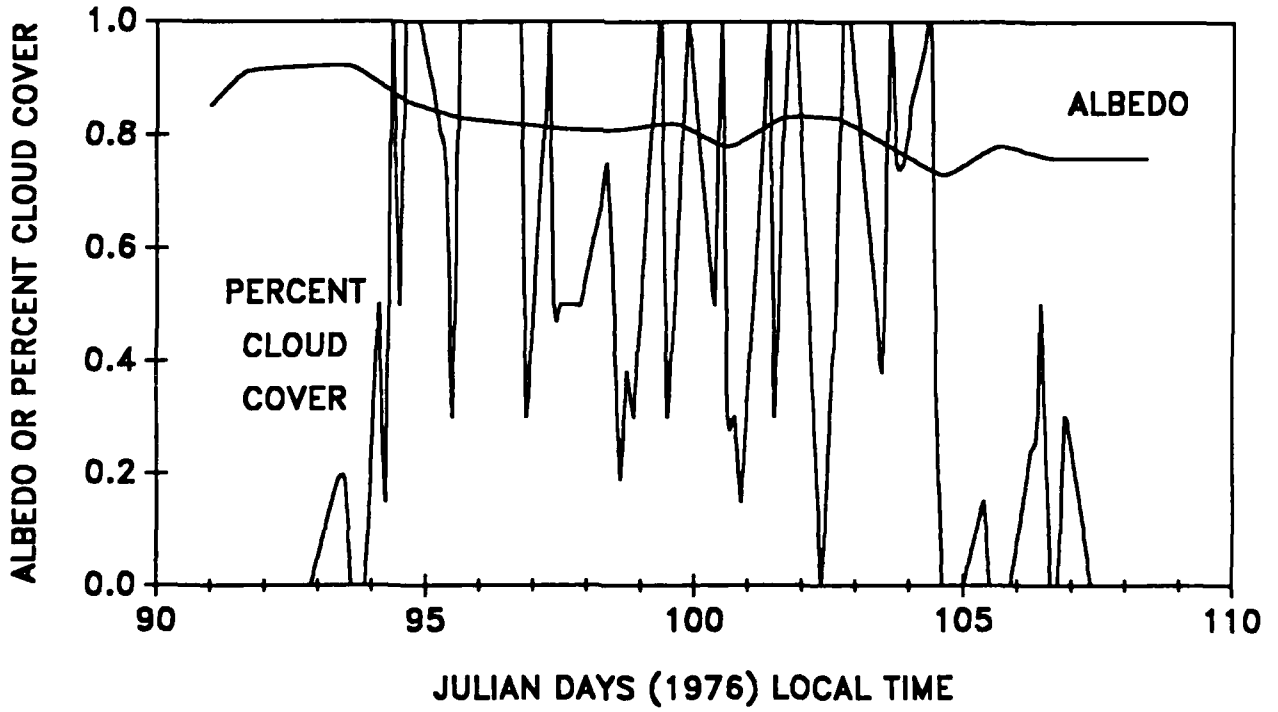

Fig. 9. Average albedo and estimated percent cloud cover for the central Beaufort Sea during April 1976.

Our numerical simulations have shown us the various modes of response of pack ice to solar and atmospheric heat fluctuations. The results can be summarized as follows. Most of the surface heat balance is between radiational heat fluxes (shortwave solar radiation in, longwave atmospheric radiation in, and longwave ice radiation out). Without a snow cover, the surface of the ice responds almost immediately to reductions in cloud cover or air temperature by significant drops in temperature. These drops in ice temperature are greatly reduced with a snow cover. Moreover, snow cover delays the times of maximum decreases in ice temperature by 5 to 24 hrs, or longer. The significance of sensible heat flux is its transfer of heat from the atmosphere which causes the pack ice to warm as a frontal system approaches (periods of higher wind speeds). Stronger winds result in warmer pack ice, and the temperature drop in the ice is more dramatic as the front moves past. Finally, the simulation results can be used to quantify the effects of ice temperature changes induced by reductions in cloud cover, air temperature, and sensible heat flux. We see that ice temperature change due to a 15°C drop in air temperature is approximately equivalent to the change resulting from a reduction in cloud cover from 80% to 0%. When the winds diminish after the passage of atmospheric fronts, sensible heat fluxes never exceeded 10% of the radiational heat fluxes when the surface of the ice was cooling. However, temperature decreases in the ice could be enhanced by up to 50% if winds caused significant sensible heat fluxes (warming of the ice) prior to the periods of cooling.

Of course, our aim here is to use the ice heat flux model to gain insight into under-ice noise that results from thermal microfracturing. In this respect, we have shown that microfracturing will be primarily a result of radiational heat balances and, thus, air temperature fluctuations will not be a reliable noise predictor. Also, cloud cover has a significant effect on heat flux at the ice surface. A complete cloud cover may insulate the ice to such a degree that microfracturing as a result of other heat fluxes might not occur. This makes the development of a correlate for non-summer, higher frequency noise a difficult task. Finally, snow cover explains why peaks in under-ice noise levels might be delayed anywhere from 5 to 24 hours. This too contributes to the difficulty in developing a correlate for higher frequency noise. For a given location, the time delay as well as the magnitude of the ambient noise will vary as snow accumulates and then, possibly, redistributes with the wind.

We now make a comment concerning the category 2 episodes that are depicted in Fig. 1 and Fig. 3 (Episode 4). These are some of the most interesting episodes thus far considered by the authors for a number of reasons:

1) First, the ice kinematic parameters indicate that these episodes were not a result of large-scale ice motion. Yet there are corresponding 15 dB anomalies in the 32 Hz record and a hint of anomalies in the 10 Hz record (Fig. 1).

2) The corresponding air temperature data indicates a temperature decrease for the times of these episodes, but then there are similar decreases which do not correspond to any noise episodes. More importantly, such noise generation due to heat fluxes are not expected to be responsible for the anomalies in the 32 Hz and 10 Hz data.

3) Since the low frequency data indicate the possibility of ice motion, one might expect that we are observing an isolated phenomena (e.g., an oceanic eddy traversing under the ice). However, the spatial structure and the duration of the episode shows that it started in the northwestern Beaufort Sea and affected the south-central Beaufort Sea within a matter of 3 to 6 hrs. Thus, its speed and spatial extent is far too great to be an isolated phenomena.

In investigating these anomalies, we considered the possibility of noise generation as a result of vertical ice motion. The spatial atmospheric variations were used to calculate the time history of vertical speed and acceleration of an ice layer. This was done using static head conditions to estimate the inverted barometer effect (higher water levels in the presence of lower atmospheric pressure). However, there was no apparent relationship between the calculated vertical speed or acceleration of the ice and the 1000 Hz noise spikes. This is consistent with the results of Weber and Erdelyi[12] who concluded that ice tilt in the Beaufort Sea is primary a wind-induced phenomena, with a downward tilt in the direction of the wind. The environmental data (decreasing or light winds, following an atmospheric pressure minimum, and falling or low temperatures) leaves us with the thermal fracturing as the only

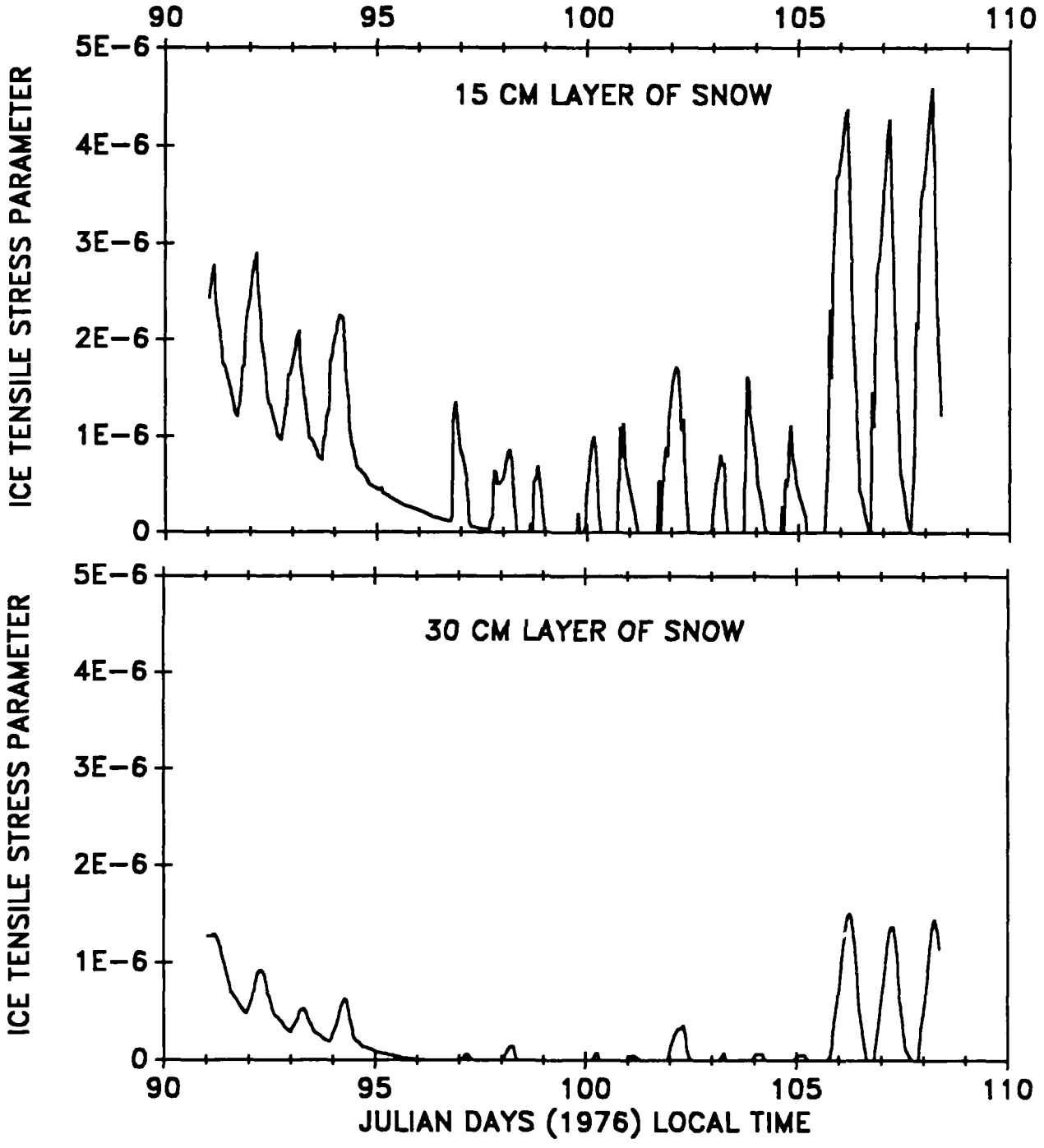

Fig. 10. Variations of the microfracturing parameter -F for simulations of heat flux in sea ice with 15 cm of snow (top) and 30 cm of snow (bottom).

explanation. But this and the 32 Hz spikes in Fig. 1 would imply that such fracturing reaches the scales of 50 m or more. As a test of this conclusion, we considered the 32 Hz noise signals of the other 1000 Hz noise anomalies. In about half the cases, the 1000 Hz anomaly had a corresponding noise spike at 32 Hz. In fact, after converting from decibels into μPa, matching diurnal variations can be readily picked out in the spring-time 32 Hz noise data (Fig. 11). Thus, one must conclude that thermal fracturing of sea ice can at times make some significant contributions to lower frequency (<150 Hz) arctic ambient noise. Considering Dyer's[13] category of thermal ice cracking for arctic ambient noise, our evidence extends the range of the category from 5000 Hz down to ~30 Hz.

8. SUMMARY AND CONCLUSIONS

We have considered higher frequency, arctic ambient noise by a number of means in this study. In particular, we concentrated on noise episodes which had no associated ice motion or wind events and the lack of noise episodes which had associated air temperature variations. These are not the only noise anomalies that caught our attention, however. We have also found distinct motion-related anomalies which show significant lowering of higher frequency noise levels under the conditions of ice pack divergence. But in most of the noise anomalies, we found thermal fracturing of the ice to be responsible. We have considered the entire suite of heating and cooling processes that relate to thermal fracturing for sea ice. This includes sensible heat flux between the ice and the air as well as solar radiation. In addition, we have studied longwave radiational heat flux from the air to the ice. The effects involved with this latter process include variations in air temperature and cloud cover.

An analytical solution to the governing equation for heat flux in ice implies that most ice fracturing will occur within the top 20 cm. With daily heat fluxes, the ice would tend to fracture well within the top 20 cm. Heat fluxes varying on the order of three to five days can be expected to produce significant thermal variations all the way down to ~45 cm. This does not imply, however, that fracturing would also reach to 45 cm.

Because of varying salt content and temperature levels, we developed a numerical model of heat flux in sea ice. From the model, we calculated an estimator of the total ice undergoing tensile stress for each time step. Simulations without any snow cover implied that sea ice tends to react rapidly to net cooling. Thus, higher frequency noise levels would tend to increase almost immediately with decreases in air temperature and/or cloud cover. In addition, maximum noise levels with a daily heating cycle were predicted to occur at 1900 hrs local. Finally, the simulations imply that sensible heat flux is of little importance in the production of higher frequency noise. Radiational heat balances are the more important factor. This is especially true since colder air temperatures and cloud-free conditions are typically associated with lower wind speeds. The primary importance of sensible heat flux is the warming of the ice before heat loss. Greater sensible heat flux during periods of warming produces warmer ice. Thus, ice fracturing (temperature drops) can be greater when cooling occurs.

Snow cover greatly changes the results of the simulations. The magnitudes of the fracturing parameter are reduced, and the implied time of maximum noise levels occurs well after the initiation of surface heat losses. With snow cover, we found that a daily heating cycle produces maximum fracturing at 0300 to 0800 hrs local. This delay is a common feature seen in the observed noise data.

Using the snow-covered model, we simulated spring time noise levels for a period in 1976. The model was forced using observed solar radiation, air temperature, wind speed, albedo, and cloud cover. The agreement of the model ice fracturing parameter and the observed 1000 Hz noise levels is quite encouraging. However, the data and the model results indicate that blowing snow and ice fog may be additional factors in the heat flux balance of sea ice.

The results of our work go a long way in explaining the nature of higher frequency arctic ambient noise. The short space scales of such noise are likely a result of spatial variations in snow cover. The short time scales of higher frequency noise are not only a result of multiple noise-generating processes but also

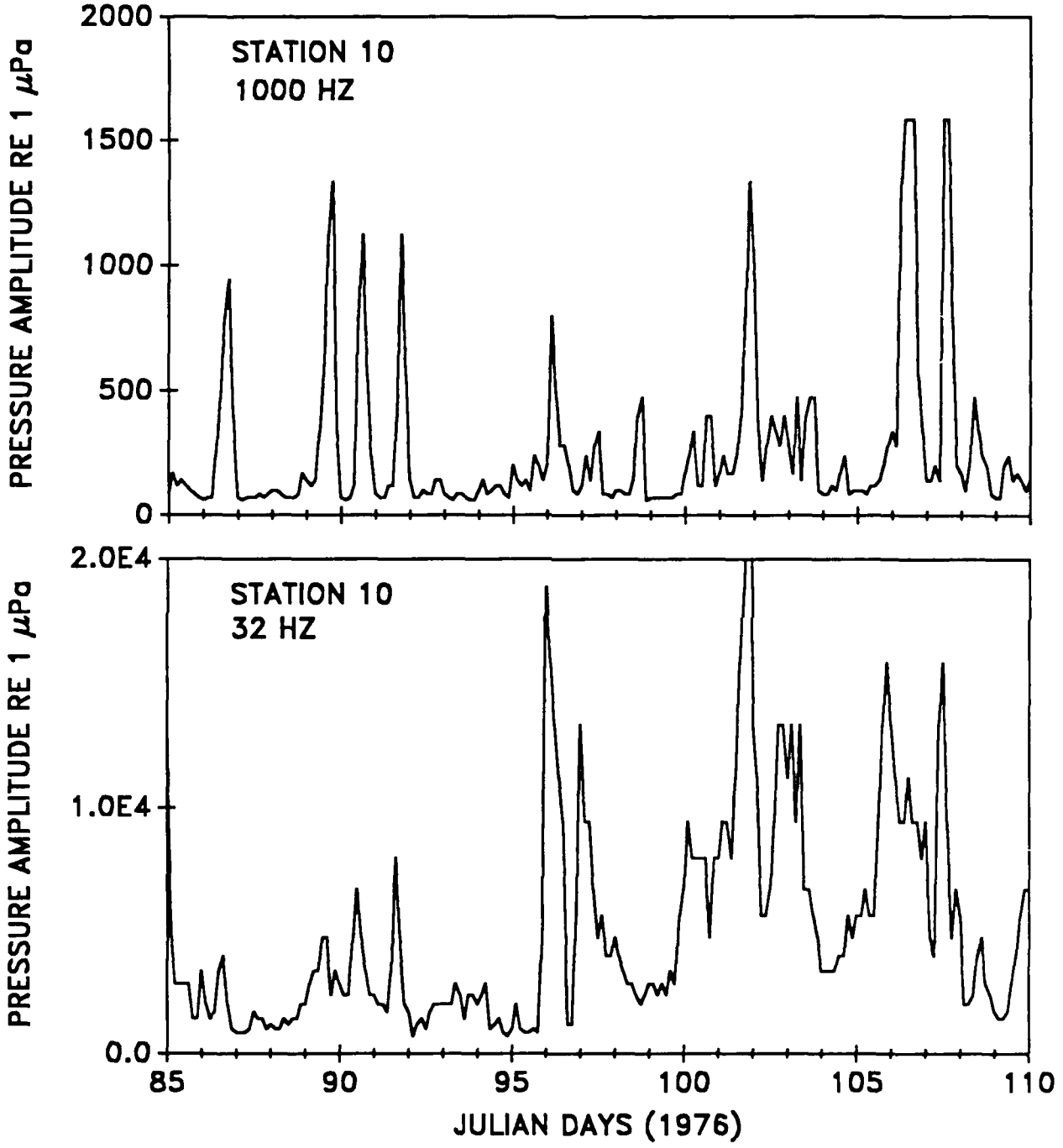

Fig. 11. Variations of the spring 1976 1000 Hz and 32 Hz noise levels. Note that the 32 Hz noise often has spikes which correspond to the diurnal 1000 Hz noise spikes.

variations in cloud and snow cover. Finally, our results indicate that fracturing of sea ice can produce broad-band noise down to at least 32 Hz.

From the results of this research, it appears that the next step in higher frequency, arctic ambient noise research is a complete suite of model simulations for different environmental scenarios. These simulations would provide the basis of an experimental design for a validation experiment. The following is suggested:

1) Incorporate ice mechanics into the numerical heat flux model. The parameters to be included would be the coefficient of thermal expansion (a function of temperature and salinity) and the Poisson ratio for ice (a function of salinity). This would allow for the direct calculation of tensile and compressive forces as a function of time and position within sea ice. Thus, the proxy variable F would be replaced with a more reliable microfracturing predictor.

2) Perform a parametric study to determine what factors are important for thermal fracturing under various conditions. This work would use combinations of wind speed, cloud cover, solar radiation levels, air temperature, ice thickness, and snow cover. The main intent here is to establish expected levels of fracturing for a wide range of conditions in the arctic. Suggested variable values are

wind speed - 0, 4, and 10 m/s
cloud cover - 0, 75, and 100%
solar radiation - 0 and 400 W/m² with daily oscillations
air temperature - -20°±5°C, 5°±5°C, slow oscillations (3 to 5 days), daily oscillations
ice thickness - 0.3, 1.2, 2.4 m
snow cover - 0, 15, and 45 cm.

3) Perform a number of non-equilibrium runs which simulate the passage of atmospheric frontal systems. This task would use logical combinations of wind speed, cloud cover, solar radiation, air temperature, ice thickness, and snow cover. Again, we wish to establish the expected levels of fracturing for various conditions found in the arctic. The parameters would be varied over an approximately 4 day cycle. We would simulate fall and winter conditions (no solar radiation) as well as spring conditions.

4) The results from 2 and 3 can be used to quantify the important factors as to sea ice fracturing. This would be done by ice thickness, air temperature, and season. Verification of some of the results would be performed using the 1000 Hz noise data collected during AIDJEX. At this point, we would investigate methods for measuring those important factors. In particular, we would look at research into determining percent cloud cover in an objective manner, determine if air temperature sensors have overcome the problem of detecting heat from the shield of the sensor, and investigate problems with the frosting of the domes of radiation sensors. The objective is to determine the best methods now available for measuring factors affecting thermal fracturing of sea ice, as well as determining manufacturers, costs, and limitations.

5) At this point, one can develop scenarios for field experiments to verify the conclusions of thermal fracturing simulations. These scenarios would include the team of scientists who would participate in the field experiment. Also, tentative sites for the experiment(s) would be determined. It would seem that a lake or bay experiment might be the most logical for the verification experiment. For example, Hudson Bay could provide a wide range of sea ice conditions while still being readily accessible when compared to the arctic. This accessibility would allow scientists to man field positions cheaply, quickly, and repeatedly to take advantage of varying environmental conditions. Moreover, one might take advantage of the assistance of the Canadian government in terms of scientists and funding.

ACKNOWLEDGEMENTS

This work was supported by the Office of Naval Research, Arctic Branch, under a contract to Science Applications International Corporation. The authors wish to thank Dr. Ira Dyer for his critical review and comments on this manuscript.

REFERENCES

1) Makris, N. C., and I. Dyer, 1986: Environmental correlates of pack ice noise. J. Acoust. Soc. Am., 79 (5), 1434-1440.
2) Lewis, J. K., and W. W. Denner, 1987: Arctic ambient noise in the Beaufort Sea: seasonal space and time scales. J. Acoust. Soc. Am., 82, 988-997.
3) Lewis, J. K., and W. W. Denner, 1988: Arctic ambient noise in the Beaufort Sea: seasonal relationships to sea ice kinematics. In press, J. Acoust. Soc. Am.
4) Milne, A. R., 1972: Thermal tension cracking in sea ice: a source of under-ice noise. J. Geophys. Res., 77, 2177-2192.
5) Thorndike, A. S. and J. Y. Cheung, 1977: AIDJEX measurements of sea ice motion 11 April 1975 to 14 May 1976. AIDJEX Bull. 35, 149 pp., Univ. of Washington, Seattle.
6) Pautzke, C. G., and G. F. Hornof, 1978: Radiation program during AIDJEX: a data report. AIDJEX Bull. No. 39, Univ. of Washington, Seattle, 165-185.
7) Maykut, G. A., 1986: Surface heat and mass balance. In Geophysics of Sea Ice (N. Untersteiner, ed.), Chap. 5. NATO ASI Series, Series B: Physics, Vol. 146. Plenum Press, New York, 395-463.
8) Maykut, G. A., and P. E. Church, 1973: Radiation climate of Burrow Alaska, 1962-1966. J. Appl. Met., 12, 620-628.
9) Schwarz, J., and W. F. Weeks, 1977: Engineering properties of sea ice. Glaciology, Vol. 19, No. 81, 499-531.
10) Untersteiner, N., 1961: On the mass and heat budget of arctic sea ice. Archiv für Meteorologie, Geophysik und Bioklimatologie, A, 12, 151-182.
11) Pounder, E. R., 1965: The Physics of Sea Ice. Pergamon Press, New York. 151 pp.
12) Weber, J. R., and M Erdelyi, 1976: Ice and ocean tilt measurements in the Beaufort Sea. J. Glaciology, 17 (75), 61-71.
13) Dyer, I., 1984: The song of sea ice and other Arctic Ocean melodies. In Arctic Policy and Technology (I. Dyer and C. Chryssostomidis, eds.). Hemisphere, New York. 11-37.

END

DATE

FILMED

6-1988

DTIC